NACA RM A58F17

NACA

RESEARCH MEMORANDUM

STATIC AND DYNAMIC-ROTARY STABILITY DERIVATIVES OF AN AIRPLANE MODEL WITH AN UNSWEPT WING AND A HIGH HORIZONTAL TAIL AT MACH NUMBERS OF 2.5, 3.0, AND 3.5

By Bedford A. Lampkin and Phillips J. Tunnell

Ames Aeronautical Laboratory
Moffett Field, Calif.

NATIONAL ADVISORY COMMITTEE
FOR AERONAUTICS

WASHINGTON

September 26, 1958
Declassified July 11, 1961

NATIONAL ADVISORY COMMITTEE FOR AERONAUTICS

RESEARCH MEMORANDUM

STATIC AND DYNAMIC-ROTARY STABILITY DERIVATIVES OF AN AIRPLANE MODEL WITH AN UNSWEPT WING AND A HIGH HORIZONTAL TAIL AT MACH NUMBERS OF 2.5, 3.0, AND 3.5

By Bedford A. Lampkin and Phillips J. Tunnell

SUMMARY

The static and dynamic-rotary stability derivatives are presented for an airplane model having an unswept wing and a high horizontal tail as determined in wind-tunnel tests at Mach numbers of 2.5, 3.0, and 3.5.

The tail contribution to the stability derivatives varied with angle of attack which was not predicted by the simplified theoretical methods used herein. The disagreement between estimated and experimental values is largely ascribed to the effects of aerodynamic interference.

The most inaccurate prediction for the wing-body configuration was for damping in pitch and yaw (approximately 50 percent of the experimental values).

INTRODUCTION

As the flight capabilities of airplanes are increased to higher supersonic speeds, the required dynamic stability is increasingly difficult to provide. Thus an understanding of the contribution of the various components of an aircraft to the over-all dynamic characteristics becomes of importance. Several reports (refs. 1, 2, 3, 4, and 5) have been published which present simplified means for estimating the rotary stability derivatives in the supersonic flight range, but little experimental data is available for checking the accuracy with which the derivatives may be estimated. The purpose of the investigation reported herein is to provide wind-tunnel data in the Mach number range from 2.5 to 3.5 for a specific configuration and to compare the measured values with those predicted by simplified theoretical methods.

The model used in this investigation was selected primarily because of the interesting study it permitted of the effects of the impingement of the expansion and compression field from the wing on the tail. The model was tested with and without the empennage tails to provide an assessment of tail contribution to the airplane stability. No attempt was made to evaluate the separate effects of the vertical and horizontal tail.

Static stability derivatives for this model or a geometrically similar model have been determined in earlier investigations and are presented in references 6, 7, and 8 for Mach numbers from 0.25 to 2.00. Dynamic stability derivatives for Mach numbers from 0.25 to 0.94 are also presented in reference 8.

The tests were conducted at Mach numbers 2.5, 3.0, and 3.5 through an angle-of-attack range of -8° to $+14^\circ$ at 0° of sideslip. The Reynolds number based on the wing mean aerodynamic chord was 1.5 million throughout the test.

In this report are presented five dynamic stability derivatives: damping in pitch, damping in yaw, rolling moment due to yawing velocity, damping in roll, and yawing moment due to rolling velocity; and three static stability derivatives: longitudinal, directional, and effective dihedral.

DEFINITIONS AND SYMBOLS

Forces and moments are referred to a body system of axes as defined in figure 1. The stability derivatives are defined as follows:

C_{L_α} $\dfrac{\partial C_L}{\partial \alpha}$

C_{Y_β} $\dfrac{\partial C_Y}{\partial \beta}$

C_{l_β} $\dfrac{\partial C_l}{\partial \beta}$

$C_{l_{\dot{\beta}}}$ $\dfrac{\partial C_l}{\partial (\dot{\beta} b/2V)}$

C_{l_p} $\dfrac{\partial C_l}{\partial (pb/2V)}$

C_{l_r} $\dfrac{\partial C_l}{\partial(rb/2V)}$

C_{m_α} $\dfrac{\partial C_m}{\partial \alpha}$

$C_{m_{\dot{\alpha}}}$ $\dfrac{\partial C_m}{\partial(\dot{\alpha}\bar{c}/2V)}$

C_{m_q} $\dfrac{\partial C_m}{\partial(q\bar{c}/2V)}$

C_{n_β} $\dfrac{\partial C_n}{\partial \beta}$

$C_{n_{\dot{\beta}}}$ $\dfrac{\partial C_n}{\partial(\dot{\beta}b/2V)}$

C_{n_p} $\dfrac{\partial C_n}{\partial(pb/2V)}$

C_{n_r} $\dfrac{\partial C_n}{\partial(rb/2V)}$

The other terms and symbols are as follows:

C_L lift coefficient, $\dfrac{\text{lift}}{(1/2)\rho V^2 S}$

C_Y side-force coefficient, $\dfrac{\text{side force}}{(1/2)\rho V^2 S}$

C_l rolling-moment coefficient, $\dfrac{\text{rolling moment}}{(1/2)\rho V^2 Sb}$

C_m pitching-moment coefficient, $\dfrac{\text{pitching moment}}{(1/2)\rho V^2 S\bar{c}}$

C_n yawing-moment coefficient, $\dfrac{\text{yawing moment}}{(1/2)\rho V^2 Sb}$

A aspect ratio, $\dfrac{b^2}{S}$

B	$\sqrt{M^2 - 1}$
M	Mach number
Q	body volume
R	Reynolds number, based on $\bar{c}$
S	wing area
S_b	body base area
S_t	tail area of pertinent component
V	velocity
b	wing span
c	local wing chord
$\bar{c}$	wing mean aerodynamic chord
i_t	incidence angle of horizontal tail
l	body length
l_h	length from body moment reference to horizontal-tail center of pressure
l_m	length from nose of body to moment reference
l_v	length from body moment reference to vertical-tail center of pressure
p	rolling velocity
q	pitching velocity
q_∞	free-stream dynamic pressure
r	yawing velocity
x_{cg}	length from leading edge of $\bar{c}$ to axis of rotation
x_{cp}	length from leading edge of $\bar{c}$ to center of pressure
y	distance measured along the wing span

$\bar{y}$ distance of centroid of wing area from the x axis

z vertical distance from aerodynamic center of vertical tail to fuselage reference line

Γ dihedral of the wing, deg

α angle of attack, radians except where noted

β angle of sideslip, radians except where noted

ϵ downwash angle at the tail, radians

η tail efficiency factor, $\frac{\text{dynamic pressure at the tail}}{\text{free-stream dynamic pressures}}$

ρ density

σ sidewash angle at the tail, deg

$(\dot{})$ $\frac{d(\)}{dt}$

MODEL

The complete model consisted of an unswept wing of aspect ratio 2.44, a horizontal tail mounted high on a vertical tail and a circular body modified by the addition of a canopy and simulated side inlets. A three-view drawing of the model showing the important dimensions and photographs of the model mounted on the oscillation apparatus in the tunnel are presented in figures 2 and 3, respectively. Additional geometric and dimensional characteristics of the model are given in table I.

The model was built of a magnesium alloy and weighed approximately 15.7 pounds. Model weight was kept at a minimum to obtain the desired oscillation frequency of the apparatus and to lessen vibration problems inherent in this type of testing. A more complete description of the model construction details is given in reference 8.

APPARATUS

Tests were conducted in the 8- by 7-foot supersonic test section of the Ames Unitary Plan Wind Tunnel. This wind tunnel is capable of continuous variation of Mach number from 2.5 to 3.5 and of stagnation pressures from 2 to 28 psia. A more detailed description of the wind tunnel may be found in reference 9.

The stability derivatives were measured by means of a single degree of freedom oscillation apparatus and such auxiliary electronic equipment as required to establish a steady-state forced oscillation of the model and to measure the moments and amplitudes within the balance. The oscillation apparatus and computing equipment are described in detail in reference 10.

During the first period of the test, data from the strain-gage measurements were indicated on deflection galvanometers with an observer manually recording all data. For the latter portion of the test the data were automatically recorded with three values of the oscillatory quantities being recorded and processed through a digital computer to obtain the stability derivative. The difference in the accuracy of the two methods was within the random scatter of the data.

TESTS

Tests were made at Mach numbers of 2.5, 3.0, and 3.5 through an angle-of-attack range of -8° to $+14^{\circ}$ with the sideslip angle remaining nominally zero and at a Reynolds number of 1.5 million.

A single set of spring flexures was used; the oscillation frequency ranged from approximately 2 to 7 cycles per second. The maximum oscillation amplitude was approximately $\pm 2^{\circ}$. At most test positions data were taken at the maximum oscillation amplitude obtainable and again at an amplitude of approximately one-half the maximum. The variation of the data was within the random scatter.

To aline more closely the trim position of the model and the angle of attack of the support tube and allow larger oscillation amplitudes about the pitch axis, the horizontal tail was attached to the model at various incidence angles. The incidence angles were $+4^{\circ}$, 0°, and -4°.

Correction to Data

Corrections to the measured values of the damping coefficients due to internal damping of the oscillation mechanism were determined from wind-off measurements of the damping with tunnel evacuated to approximately 5 inches of mercury. These tare measurements were taken prior to each start of the tunnel, and during the ensuing testing period were subtracted from the data to produce a pure aerodynamic term. The application of these tare measurements changed the value of the longitudinal damping derivative by 0.1 and the lateral damping derivatives by approximately 0.07.

RESULTS AND DISCUSSIONS

The results of this investigation are presented in figures 4 through 12. The predicted values of the stability derivatives, shown in these figures, are based on linearized supersonic theory and are the sum of the values predicted for the contributing components. The equations used in calculating the derivatives are presented in the appendix. It is recognized that the methods used for predicting the derivatives contain many simplifying assumptions, the justification for which in some instances may be subject to questions; however, the methods employed yield a rapid approximation. These equations of course may be modified to include different assumptions or additional refinements as the reader may desire.

The Longitudinal Derivatives

Static longitudinal stability, C_{m_α}.- The complete model exhibited longitudinal stability throughout the ranges of angle of attack and Mach numbers considered. In figure 4 it is indicated that below 4° angle of attack, the wing-body configuration was generally unstable. The variation of C_{m_α} with angle of attack is little affected by an increase in Mach number.

The contribution of the tail to static longitudinal stability varied markedly through the angle-of-attack range. The tail contribution appeared to be most effective at two particular regions in the angle-of-attack range at each Mach number. These regions occurred at more positive angles of attack as the Mach number increased. It was noted, from a graphical analysis, that the horizontal-tail surface passes into and out of the wing shock-expansion pattern as the angle of attack is increased from low to high values. Within the wing shock-expansion pattern, the tail operates in a zone of reduced dynamic pressure, at a reduced lift curve slope, and at a greatly reduced angle of attack, the latter as the result of downwash. At the high angles of attack, the tail is in a region of essentially free-stream dynamic pressure and no downwash (ref. 11). At the higher Mach numbers, this region is entered at higher angles of attack because of the greater sweep of the wing trailing-edge shock wave.

The static pitching-moment derivative was estimated by adding the contributions of the wing, body, and horizontal tail. The theory overestimates the wing-body contribution except at the largest negative angles of attack. Equation (3) of the appendix, which defines the contribution of the horizontal tail to the pitching moment, contains the product $\eta(1 - d\epsilon/d\alpha)$. Two-dimensional wing theory (see ref. 11) would predict this product to be zero for a tail within the shock-expansion

field of the wing where $d\epsilon/d\alpha = 1$, and to approach a value of 1 outside the field where $d\epsilon/d\alpha = 0$. Thus one would expect the experimental data in figure 4 to vary between the predicted value for the wing and body and the value predicted for the complete model assuming the above product to be 1. It is apparent that $d\epsilon/d\alpha$ at the tail, which is the predominant factor in the above product, is considerably less than unity for this particular tail when it is within the shock-expansion field of the wing. When the tail is outside the influence of the wing, the experimental curve approaches the predicted value and even exceeds it at $M = 2.5$ for reasons which are not apparent.

Damping in pitch, $C_{m_q} + C_{m_{\dot{\alpha}}}$.- Positive damping is indicated in figure 5 for both the complete model and the wing-body configuration. In contrast to C_{m_α}, there appears to be no abrupt effect of the wing shock-expansion field.

Estimated values were the sum of the individual contributions of the wing, body, and horizontal tail. The wing-body configuration exhibited approximately twice the damping theory would predict at the moderate angles of attack. This effect was also noted in the damping-in-yaw data and is thus thought to be primarily attributable to the body.

The equation for the tail contribution to the damping in pitch contains the product $\eta(1 + d\epsilon/d\alpha)$. In the light of the discussion contained in the section on C_{m_α}, one would expect this product to vary between approximately 1 and 2. The predicted derivative in figure 5 for the complete model assumes the product to be 1. The agreement between the predicted and actual contribution of the tail is quite good, adding further argument to the premise that the actual ratio of $d\epsilon/d\alpha$ at the tail on this model was considerably less than unity.

The Sideslip Derivatives

Static directional stability, C_{n_β}.- This was the only derivative which for the complete model indicated instability. This instability resulted from the large decrease of the stabilizing contribution of the tail with increasing angle of attack (see fig. 6). Only the effects of the fuselage and empennage were evaluated to obtain estimated values of C_{n_β}. To estimate the contribution of the vertical tail, a two-dimensional airfoil was assumed because of the end-plate effect of the horizontal tail and fuselage.

Estimated values of C_{n_β} for the wing-body and tail contribution were both in good agreement with the experimental values at zero angle of attack. The wing-induced pressure fields beneficially affected the

vertical-tail loading at negative angles of attack while at positive angles of attack these wing pressure fields and body vortices decreased the loading on the vertical tail.

Effective dihedral, C_{l_β}.- The complete model generally exhibited a positive dihedral effect (see fig. 7). For the wing-body configuration at a Mach number of 2.5, C_{l_β} was not obtained. Data obtained at the two higher Mach numbers indicated the tail was responsible for the positive dihedral effect of the complete model. The wing-body configuration had, except for the highest angles of attack, a negative dihedral effect because of the negative dihedral of the wings.

Only the wing and empennage contributions were evaluated to estimate values of C_{l_β}. These predicted values of the wing contribution at zero angle of attack were in good agreement with the experimental values. The predicted tail contribution was appreciably less than the experimental values. This discrepancy is probably due to wing or body interference at the tail as the predicted values were calculated assuming two-dimensional flow in the region between the horizontal tail and the fuselage center line.

The Yawing Derivatives

Damping in yaw, $C_{n_r} - C_{n_\beta}\cos\alpha$.- The damping in yaw of the complete model and the wing-body configuration is shown in figure 8. The damping in yaw of the wing-body configuration was somewhat irregular with angle of attack, but the mean value of damping was little affected by the variation in Mach number. The tail contribution to damping generally increased with angle of attack; however, this contribution was progressively less at the higher Mach numbers.

The body alone was considered in predicting the damping in yaw of the wing-body configuration since the wing contribution, calculated from a method in reference 5, was negligible. The experimental values of wing-body damping in yaw were more than twice the estimated values at zero angle of attack. Equation (12) in the appendix is similar to that used to predict body damping in pitch and in both cases the experimental values of the derivative were approximately twice the predicted values.

Estimates of the tail contribution were evaluated on the assumption that the vertical tail acted as a two-dimensional airfoil. The predicted values were larger than those obtained by experiment at zero angle of attack.

Rolling moment due to yawing velocity, $C_{l_r} - C_{l_\beta} \cos \alpha$.- This derivative, presented in figure 9, is difficult to measure and in the present report is subject to a comparatively large random scatter of data. At the two lower Mach numbers the wing-body configuration values of $C_{l_r} - C_{l_\beta} \cos \alpha$ were negative while at a Mach number of 3.5 the values of the derivative were nominally zero with the variation about equal to the scatter in the data. The tail contribution to $C_{l_r} - C_{l_\beta} \cos \alpha$ was a positive increment.

The value of $C_{l_r} - C_{l_\beta} \cos$ was predicted for the wing-body configuration considering wing dihedral only. At the higher Mach number, these values agreed more favorably with the experimental values.

The predicted effect of the vertical tail was a small positive increment to $C_{l_r} - C_{l_\beta} \cos \alpha$. Generally the agreement between predicted values and experimental data improved as the Mach number increased.

The Rolling Derivatives

Damping in roll, $C_{l_p} + C_{l_\beta} \sin \alpha$.- Positive damping in roll is indicated in figure 10 for the complete model and the wing-body configuration at all angles of attack and Mach numbers with the value of the damping decreasing as the Mach number increased.

Of particular interest was the destabilizing effect of the tail at positive angles of attack. Recent investigations, such as those reported in reference 12, indicate that a body vortex type of interference may be responsible for this decrease in damping.

The estimated values of damping in roll were predicted from evaluation of the wing and vertical-tail contributions neglecting aerodynamic interference. At zero angle of attack there was good agreement between experimental and predicted values.

Yawing moment due to rolling velocity, $C_{n_p} + C_{n_\beta} \sin \alpha$.- This derivative, presented in figure 11, is also difficult to measure and the data are subject to a comparatively large amount of random scatter.

The value of this derivative for the wing-body configuration is positive at a Mach number of 3.0 and nominally zero within the random scatter at a Mach number of 3.5. Contrary to what might be expected the contribution of the tail was a negative increment.

The values of $C_{n_p} + C_{n_\beta} \sin \alpha$ for the wing-body configuration were predicted considering only the effect of wing dihedral. The estimated values for the wing-body configuration and the complete model were in poor agreement with the experimental values both as to sign and magnitude.

Variation of Static Derivatives With Mach Number

In figure 12 data are presented for the variation with Mach number of three static stability derivatives for the complete model obtained in this investigation and in other tunnels (refs. 6, 7, and 8). The mean angles of attack and sideslip of the model are zero. Variation in model geometry and test parameters contribute to disagreements in data comparison.

Static longitudinal stability, C_{m_α}.- Two values of the estimated C_{m_α} are presented in figure 12(a) in which the term, $(1 - d\epsilon/d\alpha)$, was assumed to be 1.0 and 0.5. It appears that this type of aerodynamic interference can decrease the value of C_{m_α} by more than 50 percent. This interference reaches a maximum near a Mach number of 2.5 and, from a graphical analysis, appears to be the effect of the wing shock-wave pattern.

Static directional stability, C_{n_β}.- It is shown in figure 12(b) that as the supersonic Mach number was increased the stability of the model was reduced, approaching zero at a Mach number of about 3.25.

Effective dihedral, C_{l_β}.- In figure 12(c) a positive dihedral effect was indicated throughout the Mach number range. The estimated values are consistently lower than the experimental values.

CONCLUSIONS

The static and dynamic-rotary stability derivatives of an airplane model having an unswept wing and a high horizontal tail were measured in a wind tunnel at supersonic speeds. The following conclusions are drawn from consideration of the test results.

1. Aerodynamic interference appeared to be largely responsible for the disagreement between the measured tail contribution to the various derivatives and values predicted by simplified theoretical methods.

2. The damping in pitch and yaw of the wing-body combination were approximately twice the estimated values.

3. The addition of the tail to the wing-body configuration resulted in decreased damping in roll at positive angles of attack and contributed a negative yawing moment due to rolling velocity ($C_{n_p} + C_{n_\beta} \sin \alpha$).

Ames Aeronautical Laboratory
National Advisory Committee for Aeronautics
Moffett Field, Calif., June 17, 1958

APPENDIX

EQUATIONS USED TO ESTIMATE STABILITY DERIVATIVES

The assumptions made and the equations used to obtain the estimated values of the stability derivatives shown in figures 4 through 12 are summarized herein. All equations presented are oriented about the body system of axes defined in figure 1. In these equations it is assumed that the individual contributions of the various components are directly additive. The effects of aerodynamic interference have not been evaluated and the tail efficiency factor has been assumed to be 1. In the secondary term derivative expressions, cosine α has been assumed to be unity and sine α assumed to be zero.

Estimate of C_{m_α}.- The body pitching-moment contribution was determined by the method developed in reference 13, equation (15), neglecting the viscous term. The resulting equation is given below.

$$(C_{m_\alpha})_{body} = \frac{2}{57.3} \frac{Q - S_b(l - l_m)}{S\bar{c}} \quad \text{per deg} \tag{1}$$

The wing and horizontal-tail contributions were obtained from the following equations, respectively,

$$(C_{m_\alpha})_{wing} = -(C_{L_\alpha})_{wing} \frac{x_{cp} - x_{cg}}{\bar{c}} \tag{2}$$

with

$$x_{cp} = \bar{c}/2$$

and

$$(C_{m_\alpha})_{tail} = -(C_{L_\alpha})_{tail} \frac{l_h}{\bar{c}} \eta\left(1 - \frac{d\epsilon}{d\alpha}\right) \tag{3}$$

with $\eta(1 - d\epsilon/d\alpha) = 1$ in figure 4 and $\eta(1 - d\epsilon/d\alpha) = 1$ and 0.5 in figure 12(a).

The lift curve slope values were obtained from reference 1.

Estimate of $C_{m_q} + C_{m_{\dot{\alpha}}}$.- The body damping in pitch was determined from equation (B21) in reference 2

$$(C_{m_q} + C_{m_{\dot{\alpha}}})_{body} = - \frac{4S_b}{S\bar{c}^2} (l - l_m)^2 \qquad (4)$$

The contribution of the wing given in reference 5 is

$$(C_{m_q} + C_{m_{\dot{\alpha}}})_{wing} = - \frac{2}{3B} - \frac{8}{B}\left(1 - \frac{1}{2AB}\right)\left(\frac{x_{cg}}{\bar{c}}\right)^2 + \frac{1}{3B^3}\left(2 - \frac{2+B^2}{AB}\right) - \frac{1}{B^3}\left(-4 + \frac{8+4B^2}{3AB}\right)\frac{x_{cg}}{\bar{c}} \qquad (5)$$

The horizontal-tail contribution was estimated by the following equation

$$(C_{m_q} + C_{m_{\dot{\alpha}}})_{tail} = -2(C_{L_\alpha})_{tail}\left(\frac{l_h}{\bar{c}}\right)^2 \eta\left(1 + \frac{d\epsilon}{d\alpha}\right) \qquad (6)$$

with values of C_{L_α} taken from reference 1, and $\eta(1 + d\epsilon/d\alpha) = 1$.

Estimate of C_{n_β}.- Converting the pitching moment of equation (1) to a yawing moment gave the body contribution as

$$(C_{n_\beta})_{body} = - \frac{2}{57.3} \frac{Q - S_b(l - l_m)}{Sb} \quad \text{per deg} \qquad (7)$$

and the tail contribution was computed from the relation

$$(C_{n_\beta})_{tail} = (C_{Y_\beta})_{tail} \frac{l_v}{b} \eta\left(1 + \frac{d\sigma}{d\beta}\right) \qquad (8)$$

with

$$C_{Y_\beta} = \frac{4}{B}$$

and

$$\eta\left(1 + \frac{d\sigma}{d\beta}\right) = 1$$

The two-dimensional lift curve slope was used because of the end-plate effect of the fuselage and horizontal tail. This value of the lift curve slope was applied to the area between the horizontal tail and the fuselage center line (see fig. 2).

Estimate of C_{l_β}.- The contribution of the wing was evaluated as a function of the wing dihedral such that the moment along the span of the wing would be

$$(q_\infty Sb)dC_l = C_{L_\alpha}\beta \sin \Gamma q_\infty yc\, dy \tag{9}$$

where $\beta \sin \Gamma$ is the effective wing angle of attack for small angles of sideslip and is the component of β in the plane normal to the wing plane. From integrations along the span of each wing the combined effect is given by

$$(C_{l_\beta})_{wing} = (C_{L_\alpha})_{wing} \frac{\overline{y}}{b} \sin \Gamma \tag{10}$$

with $(C_{L_\alpha})_{wing}$ assumed $4/B$.

The vertical-tail contribution was computed from the following equation.

$$(C_{l_\beta})_{tail} = -(C_{Y_\beta})_{tail} \frac{z}{b} \eta\left(1 + \frac{d\sigma}{d\beta}\right) \tag{11}$$

with $(C_{Y_\beta})_{tail}$ assumed $4/B$ and

$$\eta\left(1 + \frac{d\sigma}{d\beta}\right) = 1$$

Estimate of $C_{n_r} - C_{n_{\dot\beta}} \cos \alpha$.- Converting the body damping in pitch to damping in yaw resulted in the following equation.

$$(C_{n_r} - C_{n_{\dot\beta}} \cos \alpha)_{body} = -\frac{4S_b}{Sb^2}(l - l_m)^2 \tag{12}$$

and the tail contribution to damping in yaw is given by

$$(C_{n_r} - C_{n_{\dot\beta}} \cos \alpha)_{tail} = -2(C_{Y_\beta})_{tail}\left(\frac{l_v}{b}\right)^2 \eta\left(1 - \frac{d\sigma}{d\beta}\right) \tag{13}$$

with $(C_{Y_\beta})_{tail}$ assumed $4/B$ and

$$\eta\left(1 - \frac{d\sigma}{d\beta}\right) = 1$$

Estimate of $C_{l_r} - C_{l_{\dot\beta}} \cos \alpha$.- The contribution by the wing was assumed to be due to the negative wing dihedral. With the vertical axis

of rotation at the quarter chord, the contributing portion of the wing was aft of the midchord. The yawing velocity produced a sideslip angle on this panel of $r\bar{c}/2V$ such that, as in equation (9), the component $r\bar{c}/2V \sin \Gamma$ was the effective wing angle of attack. The moment along the span of the wing and over an area $(c/2)dy$ would be

$$(q_\infty Sb)C_{l_{wing}} = -2C_{L_\alpha} q_\infty \frac{r\bar{c}}{2V} \sin \Gamma \int_0^{b/2} y \frac{c}{2} dy \tag{14}$$

The stability derivative then reduces to

$$(C_{l_r})_{wing} = -(C_{L_\alpha})_{wing} \frac{\overline{cy}}{2b^2} \sin \Gamma \tag{15}$$

with $(C_{L_\alpha})_{wing}$ assumed $4/B$.

The vertical-tail contribution was obtained from the following equation.

$$(C_{l_r} - C_{l_{\dot{\beta}}} \cos \alpha)_{tail} = 2(C_{Y_\beta})_{tail} \frac{l_{vz}}{b^2} \eta\left(1 - \frac{d\sigma}{d\beta}\right) \tag{16}$$

with $(C_{Y_\beta})_{tail}$ assumed $4/B$ and

$$\eta\left(1 - \frac{d\sigma}{d\beta}\right) = 1$$

Estimate of $C_{l_p} + C_{l_{\dot{\beta}}} \sin \alpha$.- Values of BC_{l_p} for the wing were obtained from reference 3. These values are valid for wings of vanishingly small thickness with zero camber and with supersonic leading and trailing edges.

The values of the vertical-tail damping in roll were taken from reference 4. These values are valid for an isolated tail and have not been corrected for the effects of aerodynamic interference.

Estimate of $C_{n_p} + C_{n_{\dot{\beta}}} \sin \alpha$.- That component of the wing lift vector in the yaw plane due to wing dihedral was assumed to be the wing-body contribution to the yawing moment due to rolling. It was also assumed that this side force acted along the slightly swept midchord line and resulted in a moment about the axis of rotation with a moment arm of quarter-chord length. The yawing moment at each chordwise station is expressed by

$$(q_\infty Sb)dC_n = C_{L_\alpha} \sin \Gamma q_\infty \frac{py}{V} c \, dy \frac{\bar{c}}{4} \tag{17}$$

From integration along the wing span the expression for the derivative evolves to:

$$(C_{n_p})_{wing} = (C_{L_\alpha})_{wing} \sin \Gamma \frac{\bar{c}\bar{y}}{4b^2} \tag{18}$$

The vertical-tail contribution was computed from the following equation

$$(C_{n_p} + C_{n_{\dot{\beta}}} \sin \alpha)_{tail} = 2(C_{Y_\beta})_{tail} \frac{z l_v}{b^2} \eta \tag{19}$$

with $(C_{L_\alpha})_{wing}$ and $(C_{Y_\beta})_{tail}$ assumed 4/B and

$$\eta = 1$$

REFERENCES

1. Harmon, Sidney M., and Jeffreys, Isabella: Theoretical Lift and Damping in Roll of Thin Wings With Arbitrary Sweep and Taper at Supersonic Speeds. NACA TN 2114, 1950.

2. Tobak, Murray, Reese, David E., Jr., and Beam, Benjamin H.: Experimental Damping in Pitch of 45° Triangular Wings. NACA RM A50J26, 1950.

3. Jones, Arthur L., and Alksne, Alberta: A Summary of Lateral-Stability Derivatives Calculated for Wing Plan Forms in Supersonic Flow. NACA Rep. 1052, 1951.

4. Margolis, Kenneth, and Bobbitt, Percy J.: Theoretical Calculations of the Pressures, Forces and Moments at Supersonic Speeds Due to Various Lateral Motions Acting on Thin Isolated Vertical Tails. NACA Rep. 1268, 1956. (Supersedes NACA TN's 3373 and 3240)

5. Harmon, Sidney M.: Stability Derivatives at Supersonic Speeds of Thin Rectangular Wings With Diagonals Ahead of Tip Mach Lines. NACA Rep. 925, 1949. (Supersedes NACA TN 1706)

6. Smith, Willard G.: Wind-Tunnel Investigation at Subsonic and Supersonic Speeds of a Fighter Model Employing a Low-Aspect-Ratio Unswept Wing and a Horizontal Tail Mounted Well Above the Wing Plane - Longitudinal Stability and Control. NACA RM A54D05, 1954.

7. Wetzel, Benton E.: Wind-Tunnel Investigation at Subsonic and Supersonic Speeds of a Fighter Model Employing a Low-Aspect-Ratio Unswept Wing and a Horizontal Tail Mounted Well Above the Wing Plane - Lateral and Directional Stability. NACA RM A54H26b, 1955.

8. Buell, Donald A., Reed, Verlin D., and Lopez, Armando E.: The Static and Dynamic-Rotary Stability Derivatives at Subsonic Speeds of an Airplane Model With an Unswept Wing and a High Horizontal Tail. NACA RM A56I04, 1956.

9. Huntsberger, Ralph F., and Parsons, John F.: The Design of Large, High-Speed Wind Tunnels. NACA paper presented at AGARD Fourth General Assembly of the Wing-Tunnel Panel, AG15/p6, Seheveningen, The Netherlands, May 3-7, 1954.

10. Beam, Benjamin H.: A Wind-Tunnel Test Technique for Measuring the Dynamic Rotary Stability Derivatives at Subsonic and Supersonic Speeds. NACA Rep. 1258, 1956. (Supersedes NACA TN 3347)

11. Nielsen, Jack N.: The Effects of Body Vortices and the Wing Shock-Expansion Field on the Pitch-Up Characteristics of Supersonic Airplanes. NACA RM A57L23, 1958.

12. Nielsen, Jack N., and Kaattari, George E.: The Effects of Vortex and Shock-Expansion Fields on Pitch and Yaw Instabilities of Supersonic Airplanes. IAS Preprint 743, June 1957.

13. Allen, H. Julian, and Perkins, Edward W.: A Study of Effects of Viscosity on Flow Over Slender Inclined Bodies of Revolution. NACA Rep. 1048, 1951. (Supersedes NACA TN 2044)

TABLE I.- MODEL DIMENSIONS

Wing (basic plan form, leading and trailing edges extended to plane of symmetry)	
Span, b, ft	2.16
Area, S, sq ft	1.90
Mean aerodynamic chord, $\bar{c}$, ft	0.94
Aspect ratio	2.44
Leading-edge sweep, deg	27.00
Taper ratio	0.38
Incidence, deg	0
Dihedral, deg	-10
Airfoil section	
Forward 50-percent chord	Elliptical
Aft 50-percent chord	Biconvex
Thickness ratio	0.034
Horizontal tail	
Span, ft	1.20
Area, S_t, sq ft	0.48
Mean aerodynamic chord, ft	0.44
Aspect ratio	2.97
Taper ratio	0.31
Leading-edge sweep, deg	19.81
Length (distance between 0.25 chord points), l_n, ft	1.67
Height	0.69
Airfoil section	
Forward 50-percent chord	Elliptical
Aft 50-percent chord	Biconvex
Thickness ratio	0.05
Vertical tail (leading and trailing edges extended to body center line)	
Span, ft	0.69
Area, S_t, sq ft	0.56
Mean aerodynamic chord, ft	0.87
Aspect ratio	0.86
Taper ratio	0.37
Leading-edge sweep, deg	43.96
Length (distance between 0.25 chord point), l_v, ft	1.20
Height (fuselage reference line to $\bar{c}$), z, ft	0.29
Airfoil section	
Forward 50-percent chord	Elliptical
Aft 50-percent chord	Biconvex
Thickness ratio	
Root	0.043
Tip	0.050
Body	
Length, l, ft	4.65
Base area, S_b, sq ft	0.13
Moment reference (on body center line)	
Horizontal location (aft of leading edge on mean aerodynamic chord) $0.25\bar{c}$	

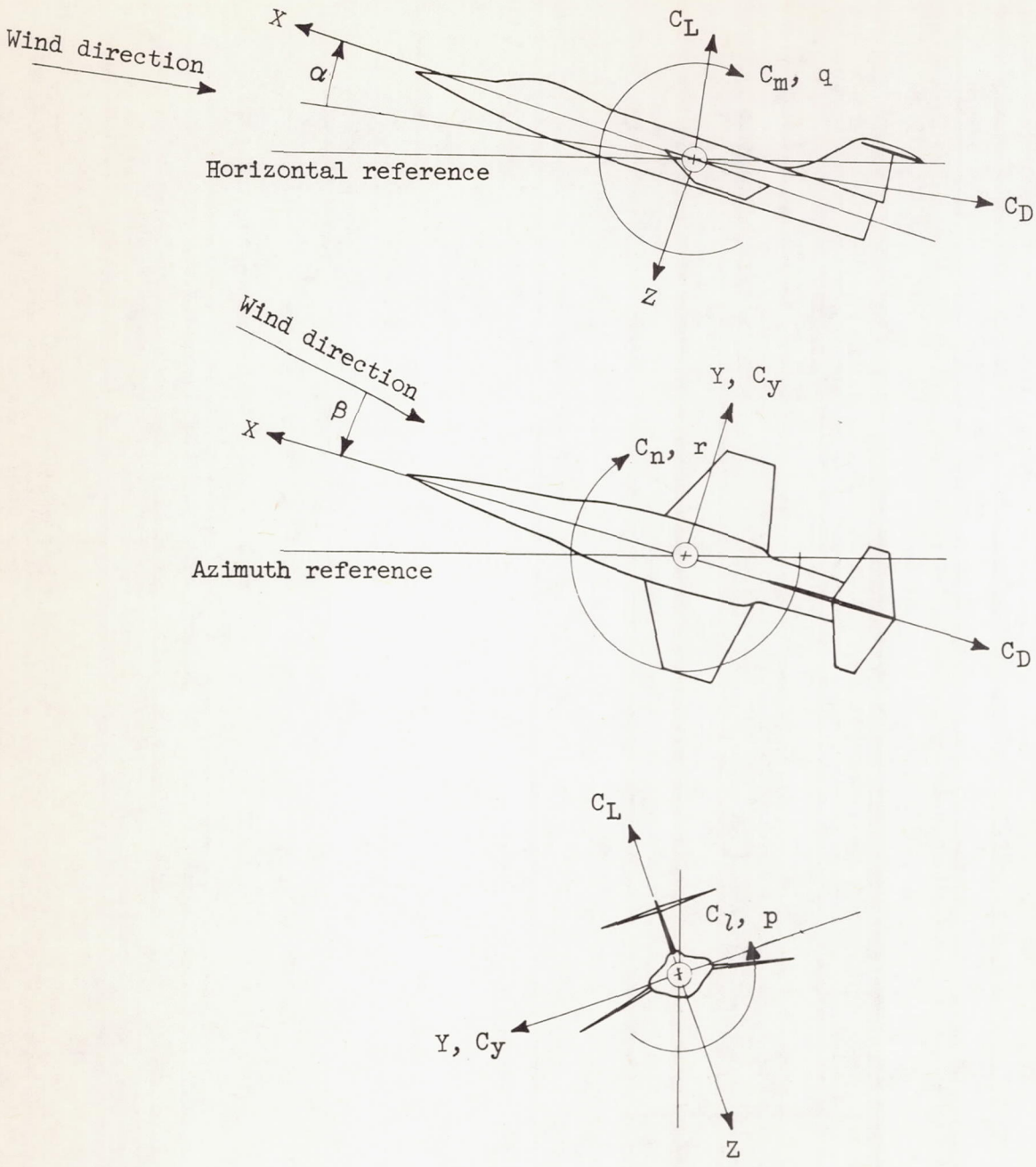


Figure 1.- The body system of axes with arrows indicating positive directions of forces and moments.

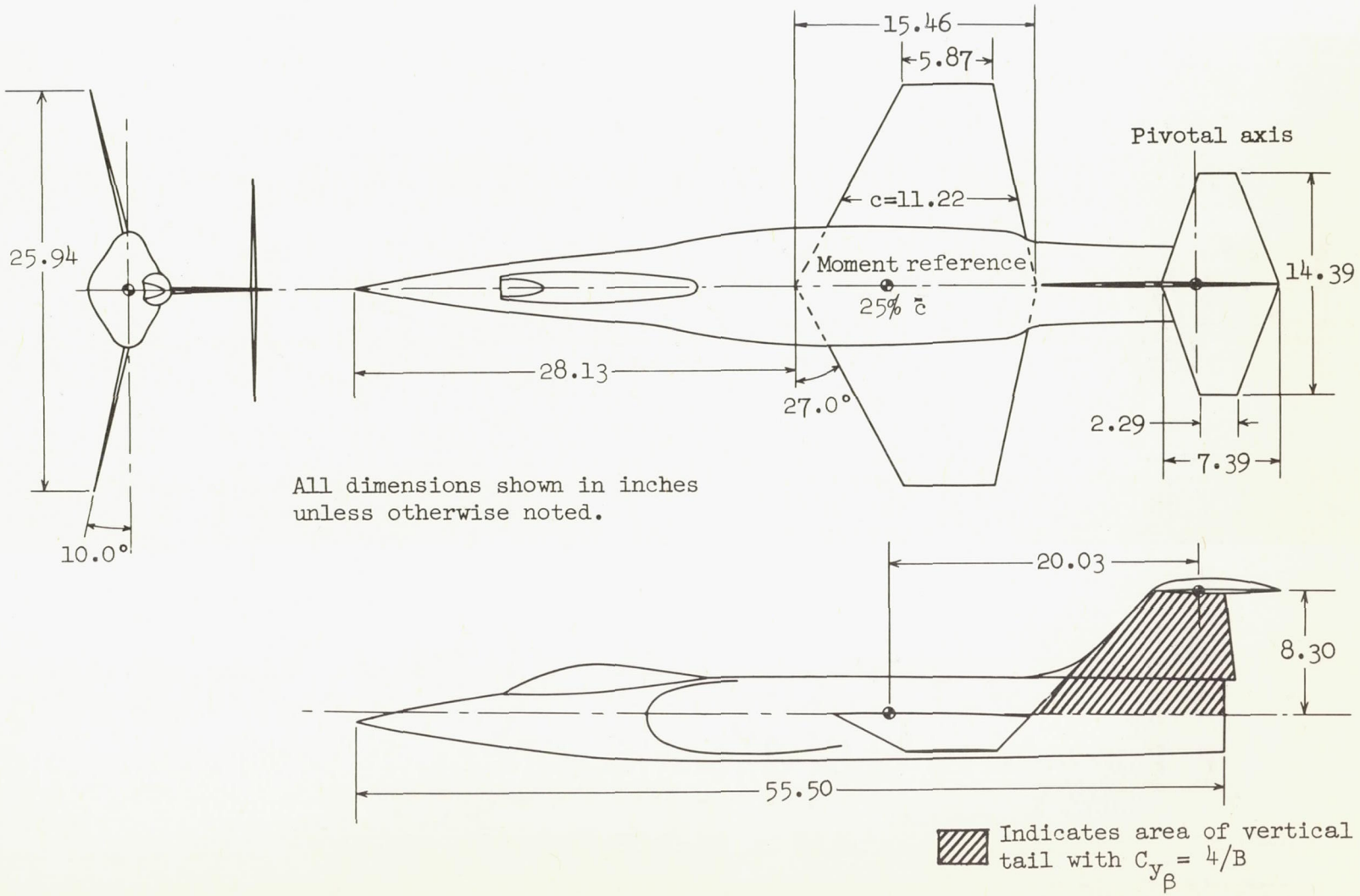
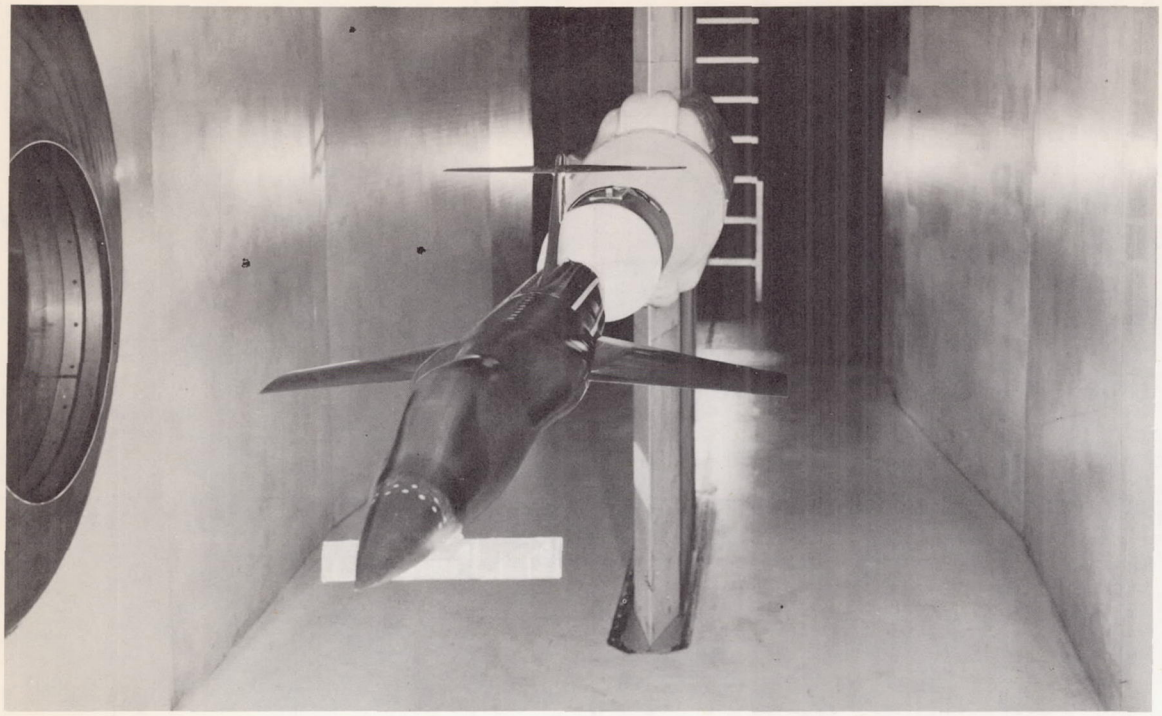
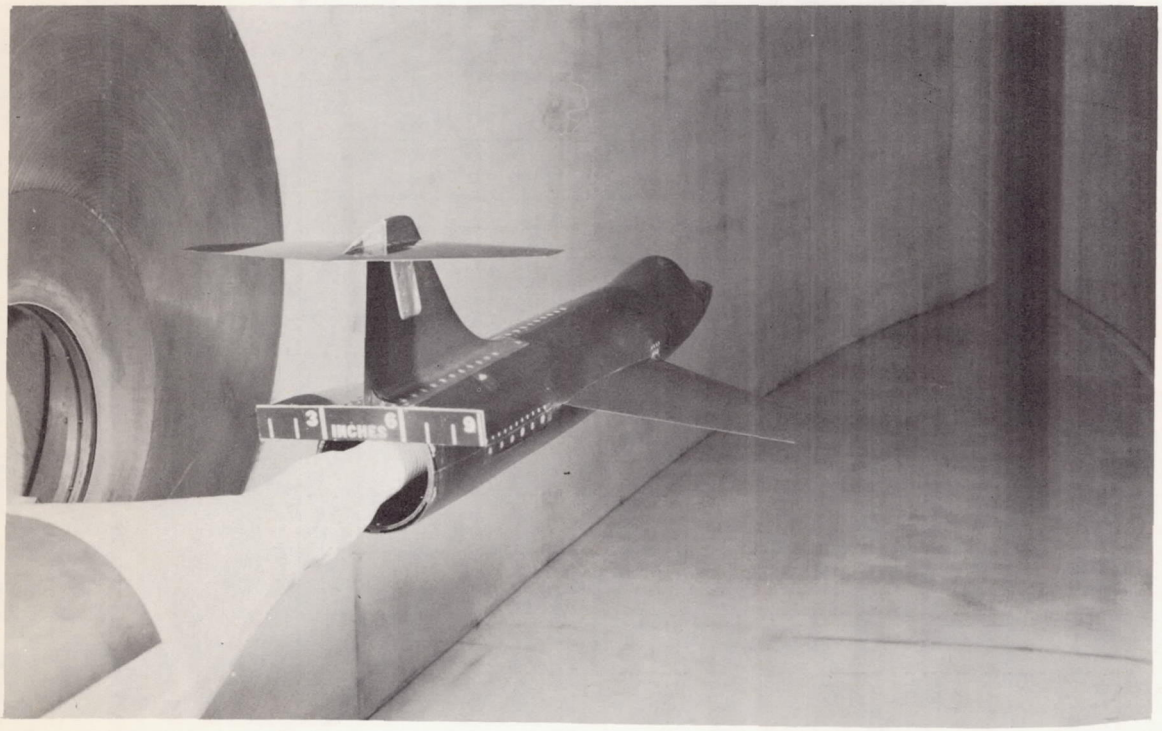


Figure 2.- Three-view drawing of the model.



A-22186



A-22187

Figure 3.- Photographs of the model mounted on the oscillation apparatus in the wind tunnel.

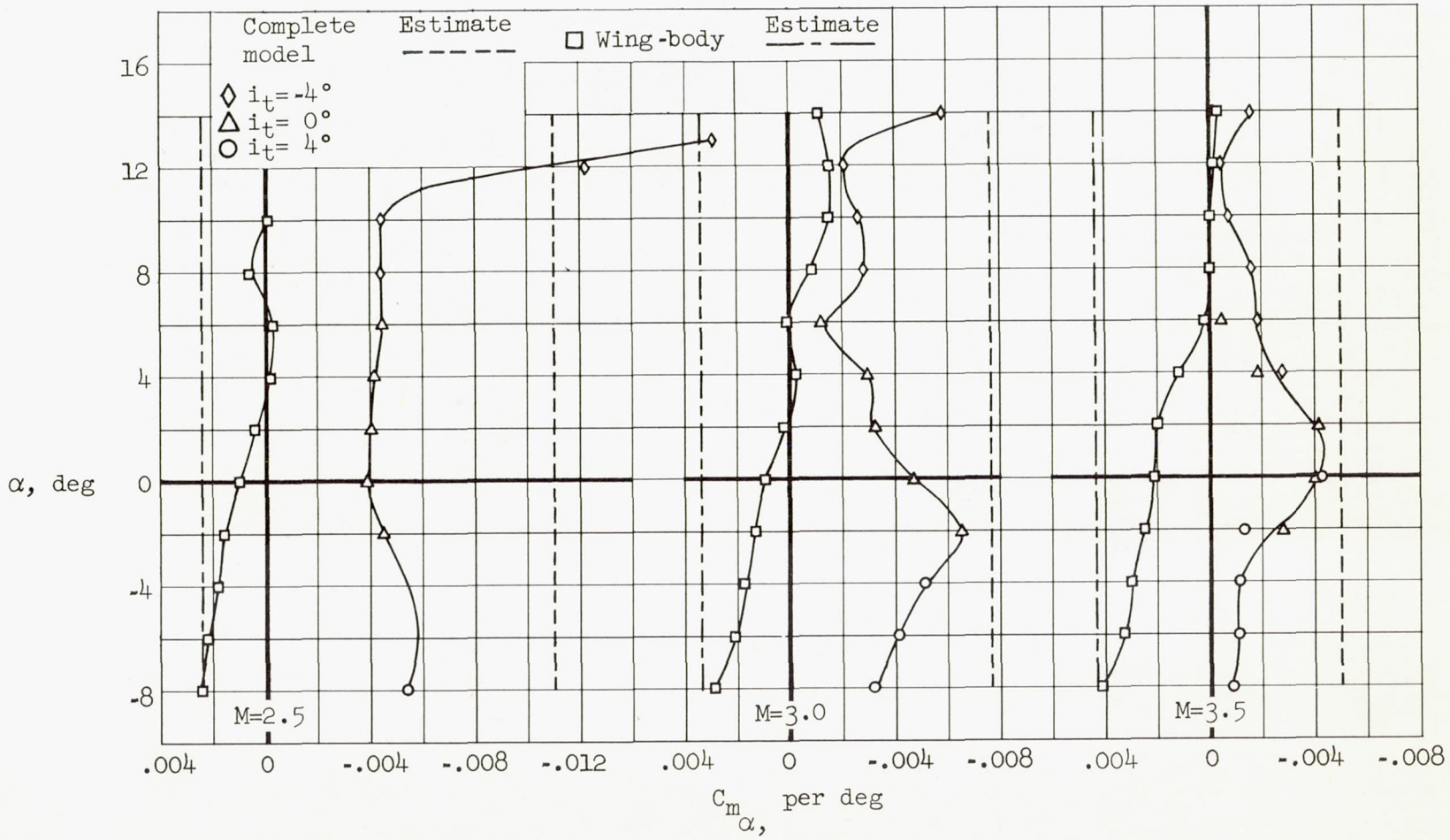


Figure 4.- The variation of the static longitudinal stability derivative with angle of attack.

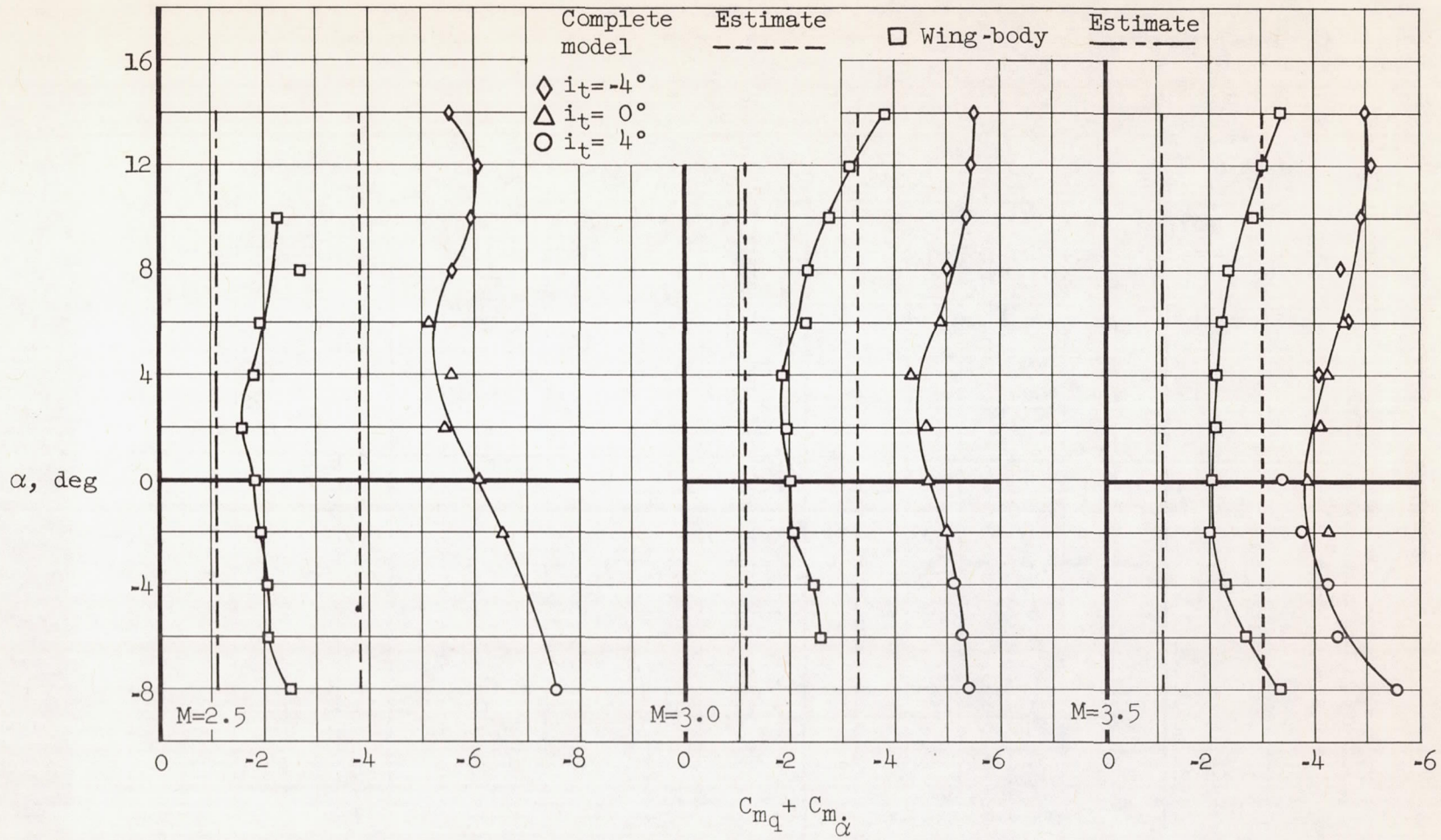


Figure 5.- The variation of the damping-in-pitch stability derivative with angle of attack.

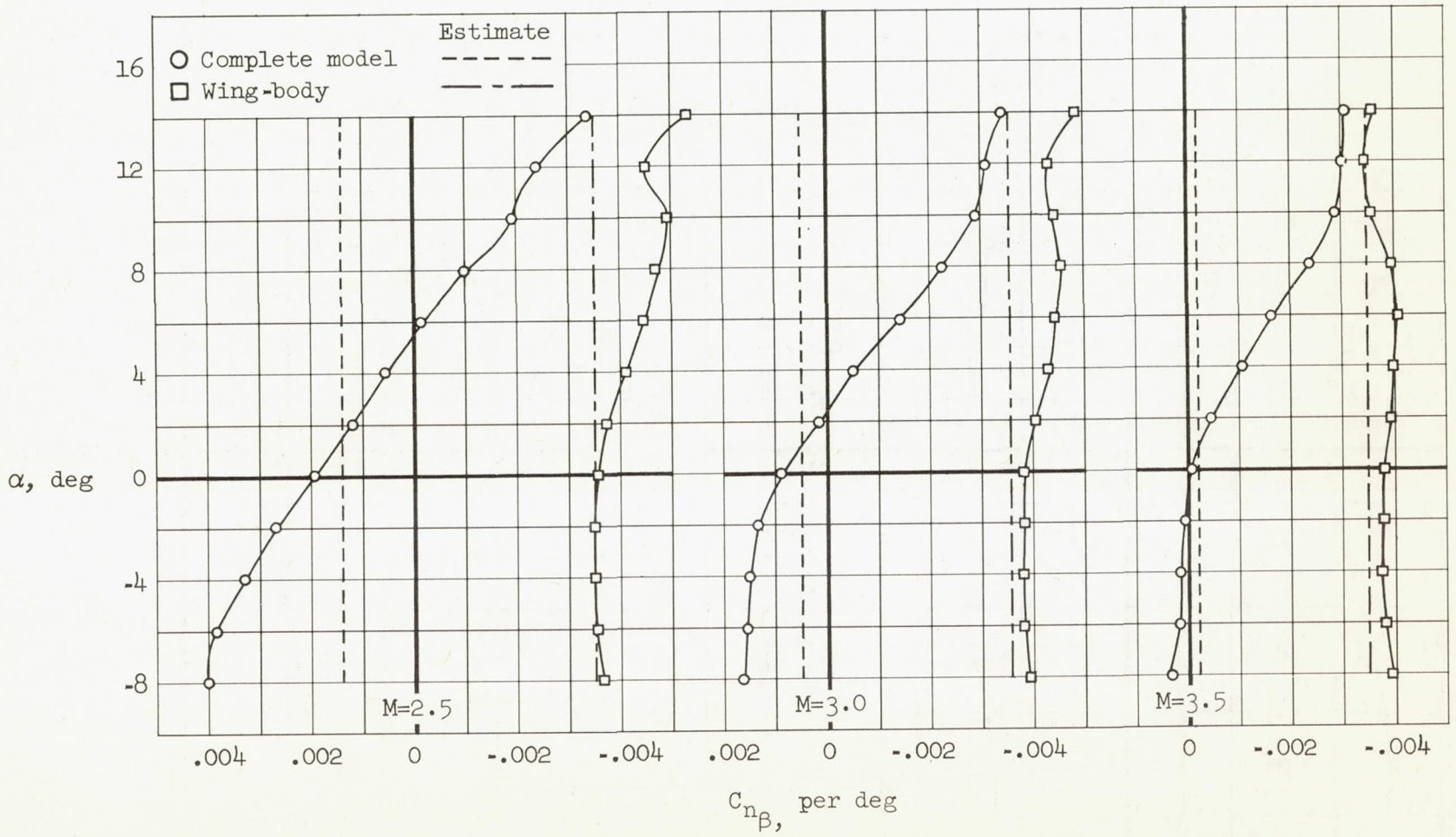


Figure 6.- The variation of the directional stability derivative with angle of attack.

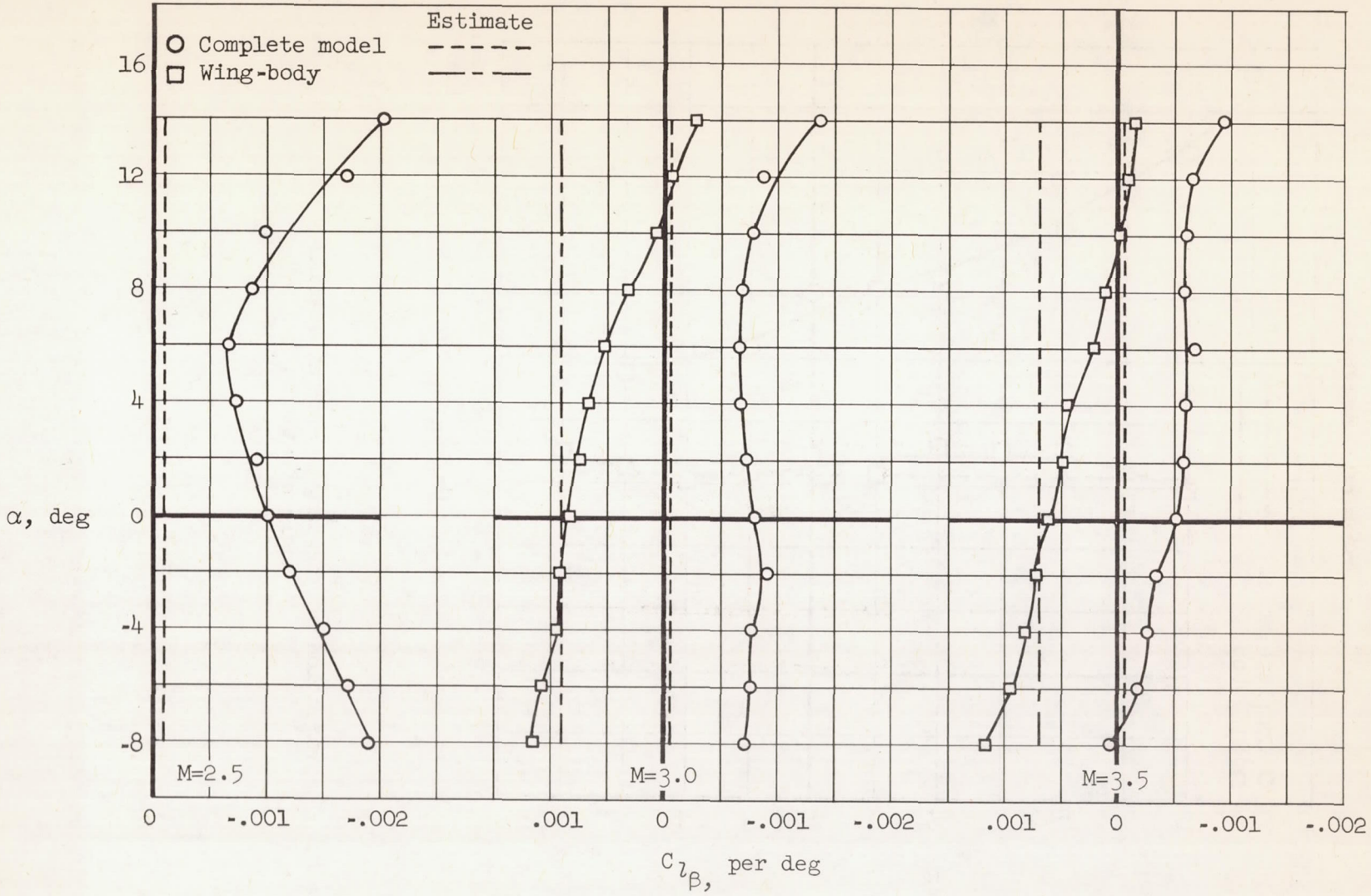
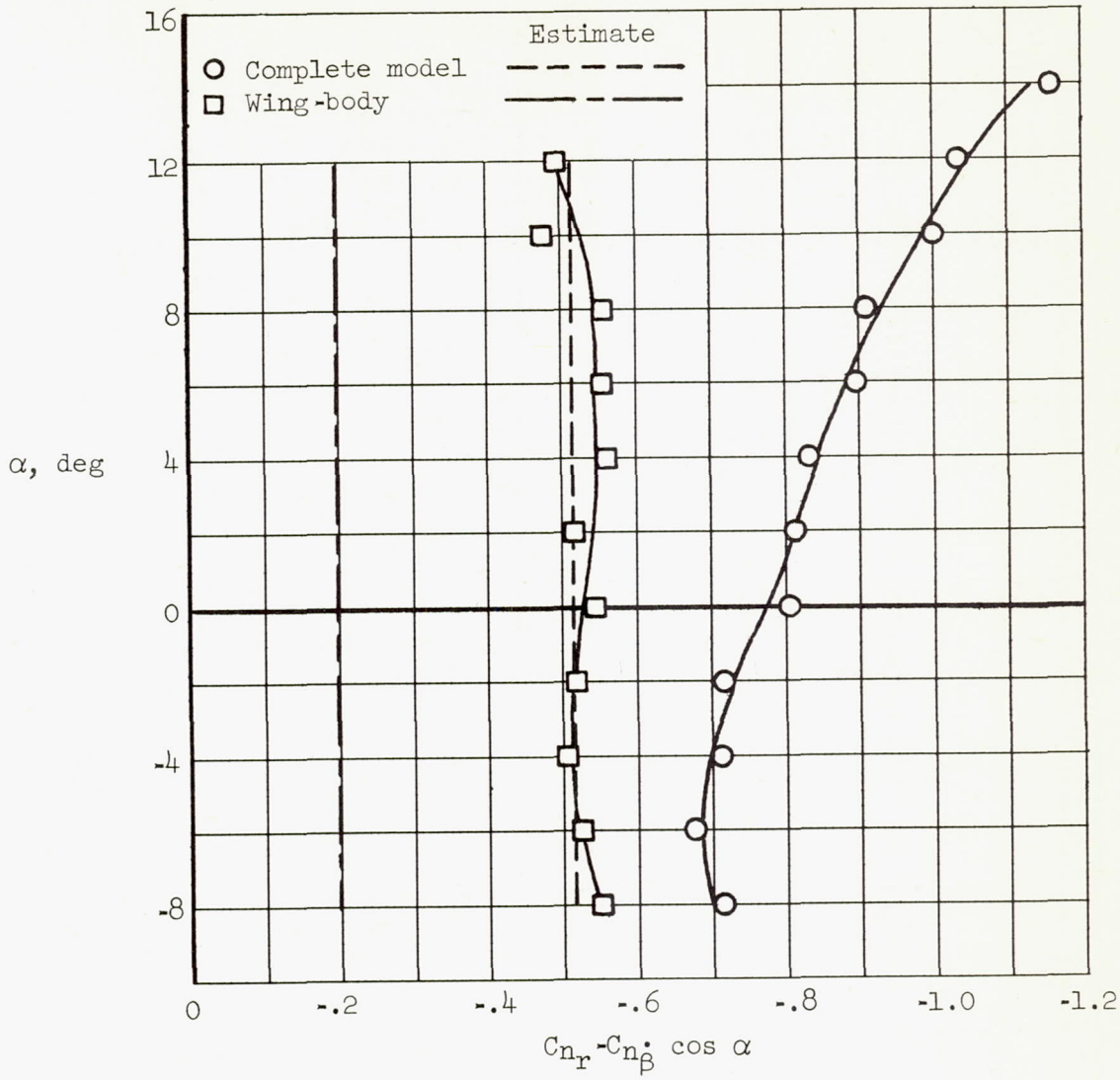
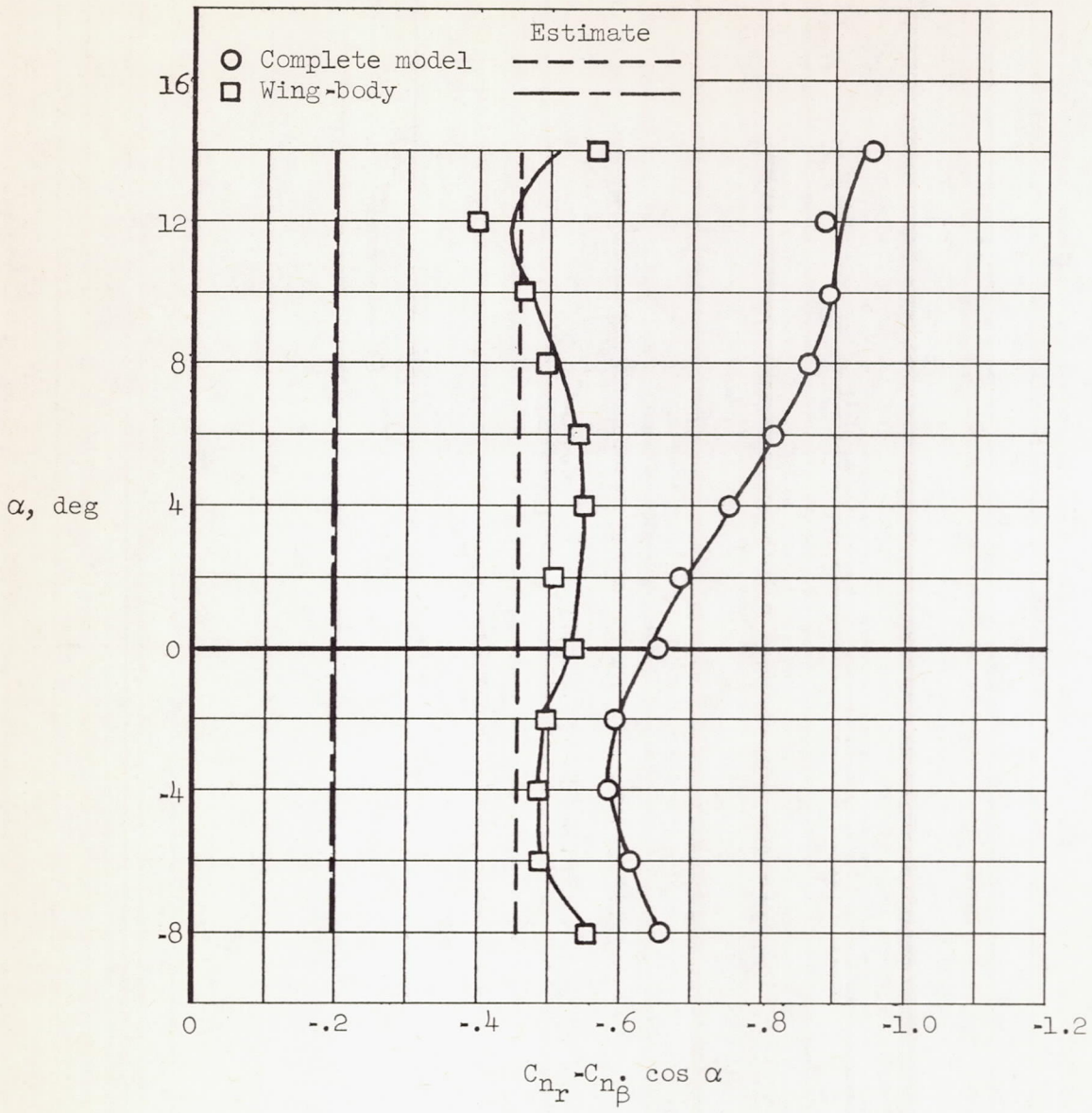


Figure 7.- The variation of the effective dihedral stability derivative with angle of attack.



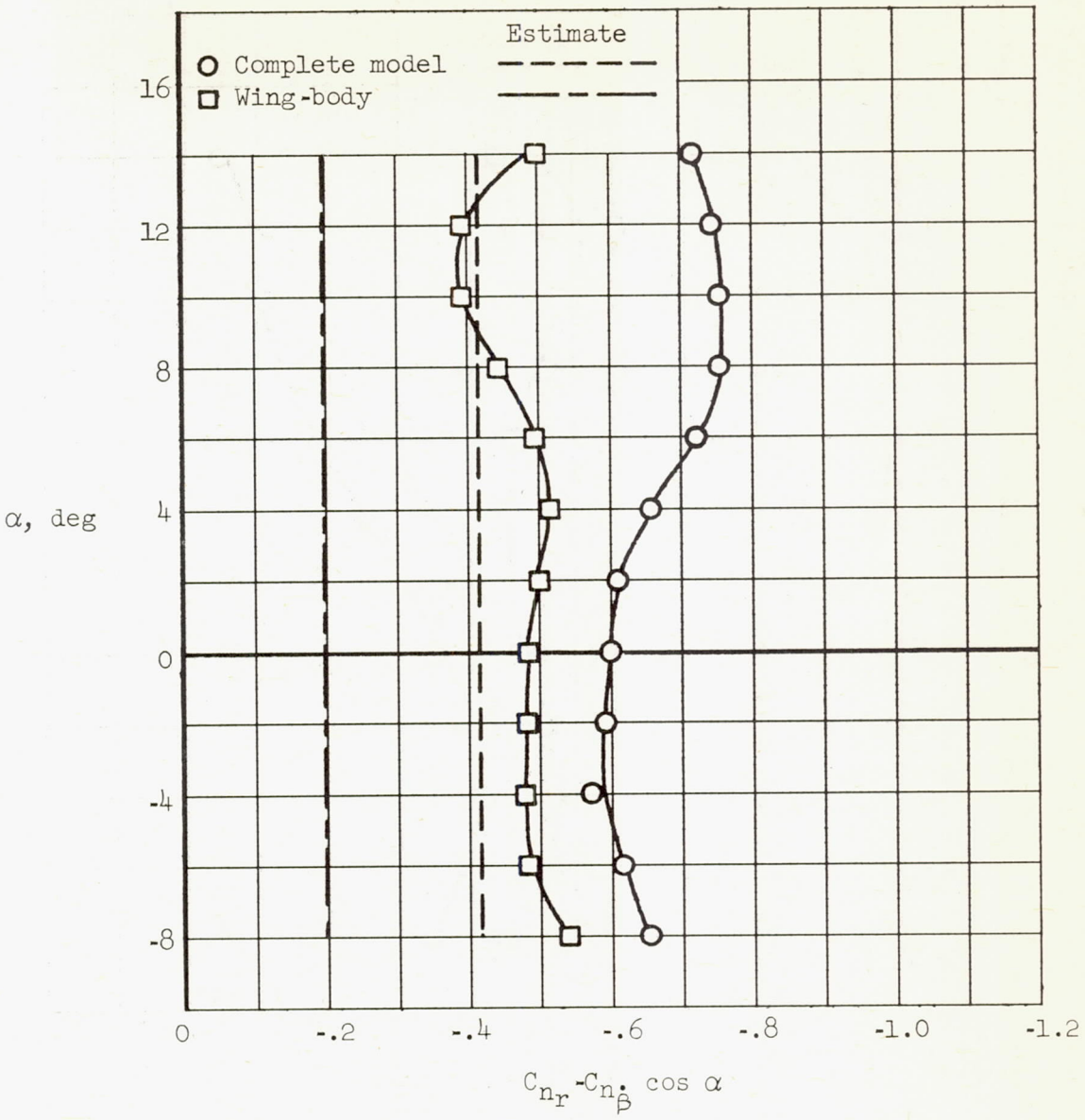
(a) M = 2.5

Figure 8.- The variation of the damping-in-yaw stability derivative with angle of attack.



(b) M = 3.0

Figure 8.- Continued.



(c) M = 3.5

Figure 8.- Concluded.

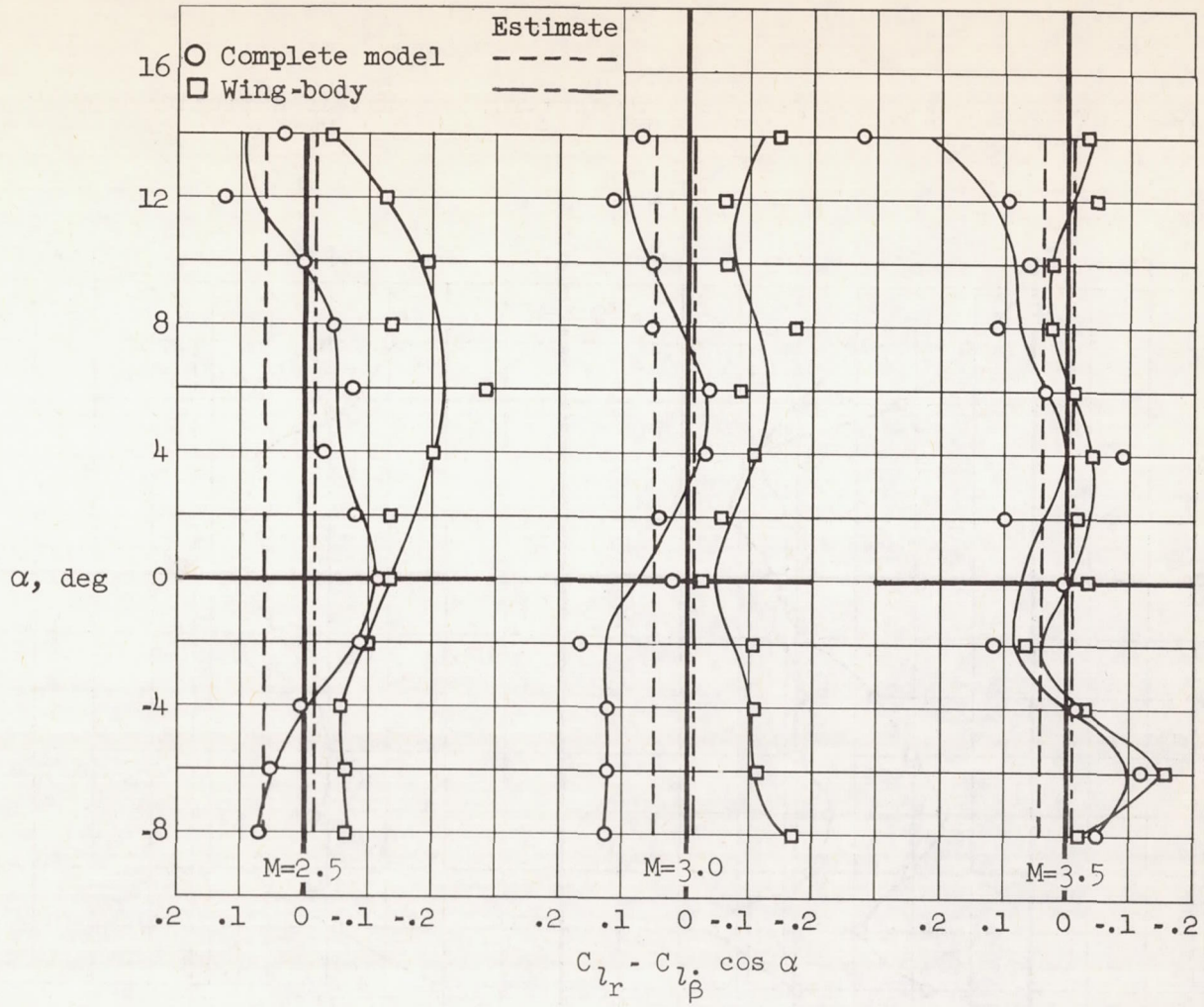


Figure 9.- The variation with angle of attack of the rolling moment due to yawing velocity stability derivative for the complete model and wing-body combination at three different Mach numbers.

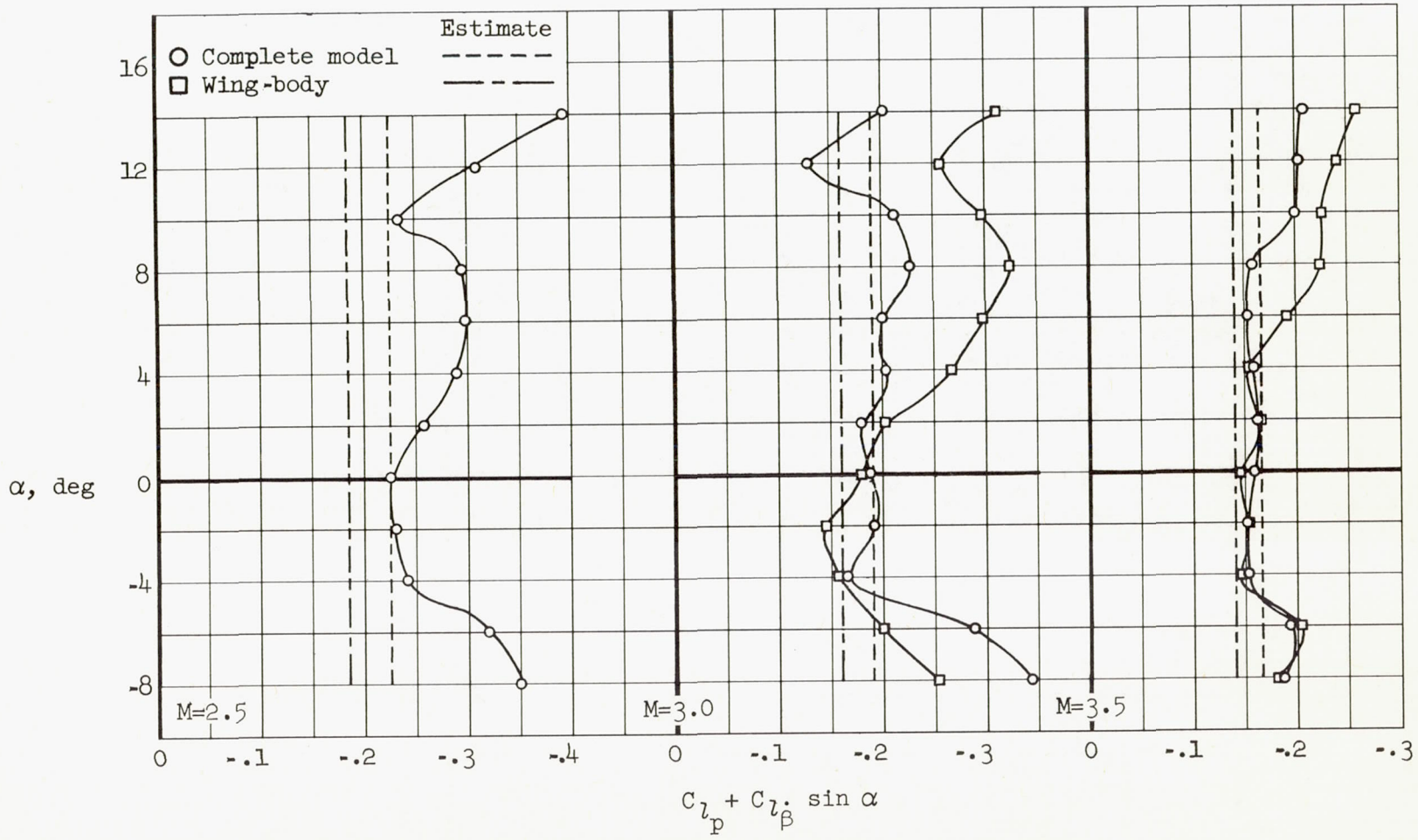


Figure 10.- The variation of the damping-in-roll stability derivative with angle of attack.

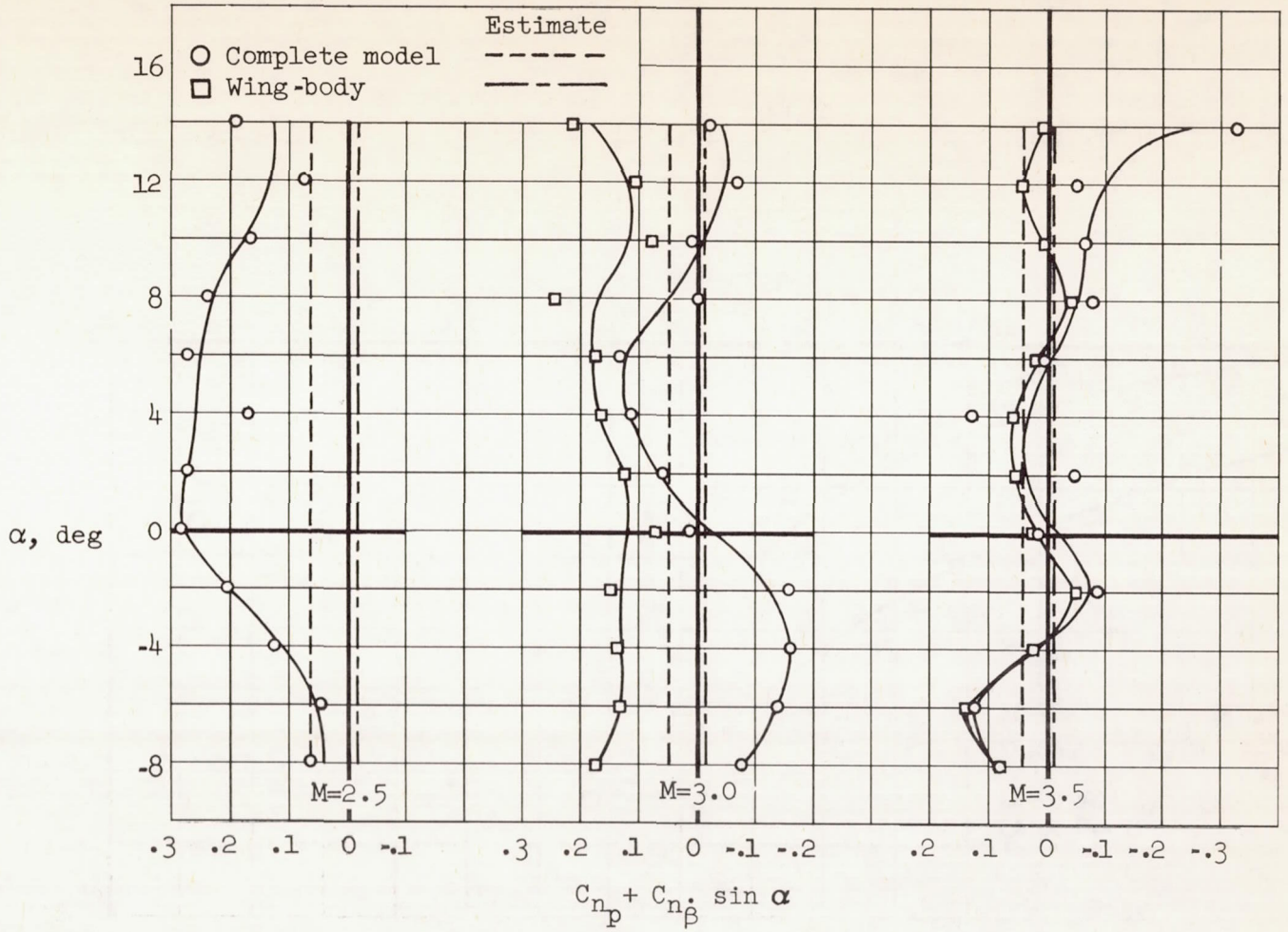
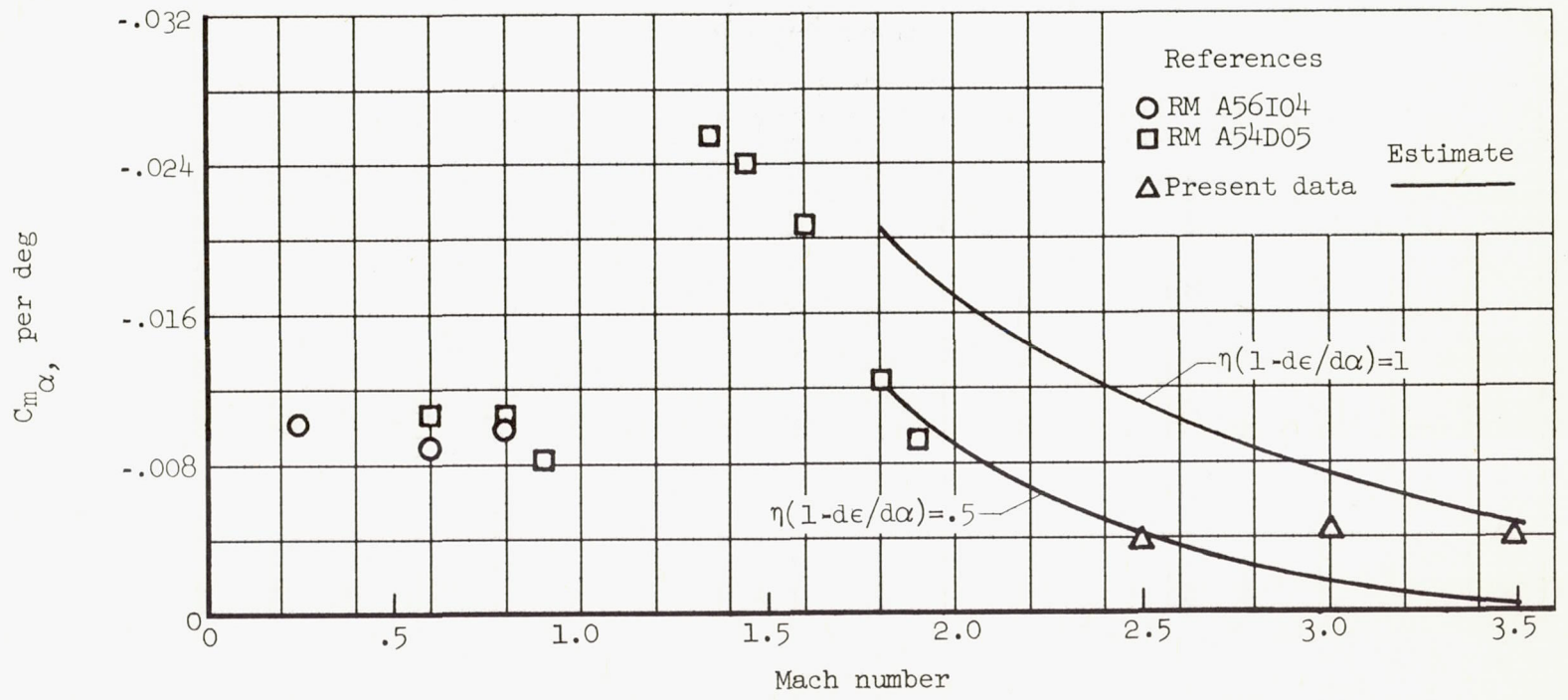
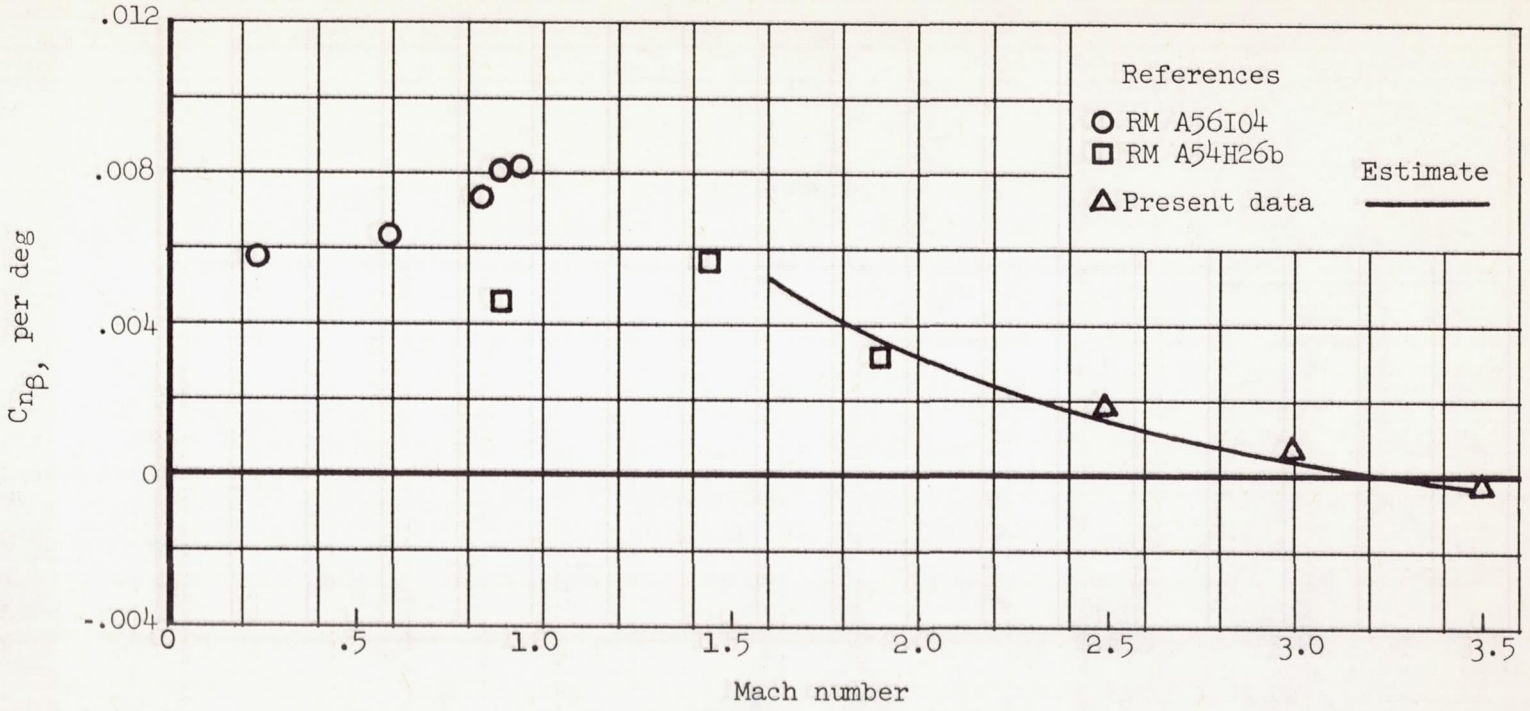


Figure 11.- The variation with angle of attack of the yawing moment due to rolling velocity stability derivative for the complete model at three different Mach numbers and for the wing-body combination at two Mach numbers.



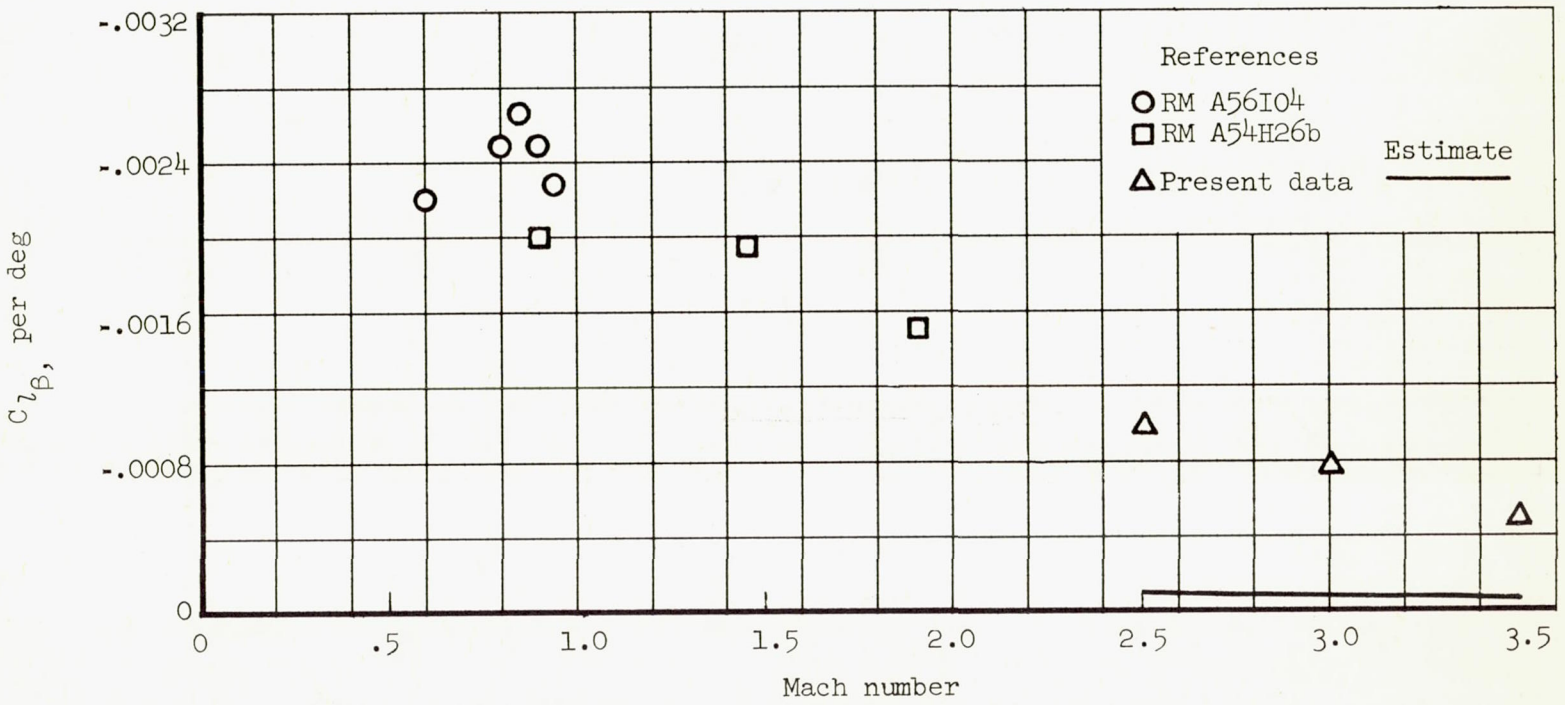
(a) C_{m_α} vs. M

Figure 12.- The variation of the static stability derivatives with Mach number for the complete model; $\alpha \approx 0$, $\beta \approx 0$.



(b) C_{n_β} vs. M

Figure 12.- Continued.



(c) C_{l_β} vs. M

Figure 12.- Concluded.

NACA - Langley Field, Va.